

Improving Dermoscopic Image Segmentation with Enhanced Convolutional-Deconvolutional Networks

Yading Yuan* and Yeh-Chi Lo

Abstract—Automatic skin lesion segmentation on dermoscopic images is an essential step in computer-aided diagnosis of melanoma. However, this task is challenging due to significant variations of lesion appearances across different patients. This challenge is further exacerbated when dealing with a large amount of image data. In this paper, we extended our previous work by developing a deeper network architecture with smaller kernels to enhance its discriminant capacity. In addition, we explicitly included color information from multiple color spaces to facilitate network training and thus to further improve the segmentation performance. We extensively evaluated our method on the ISBI 2017 skin lesion segmentation challenge. By training with the 2000 challenge training images, our method achieved an average Jaccard Index (JA) of 0.765 on the 600 challenge testing images, which ranked itself in the first place in the challenge.

Index Terms—Dermoscopic images, deep learning, fully convolutional neural networks, image segmentation, jaccard distance, melanoma

I. INTRODUCTION

MALIGNANT melanoma is among the most rapidly growing cancers in the world [1] and dermoscopy is the most commonly used *in vivo* imaging modality that provides a better visualization of subsurface structures of pigmented skin lesions [2]. While this technique allows dermatologists to detect early stage melanoma that are not visible by human eyes, visual interpretation alone is a time-consuming procedure and prone to inter- and intra-observer variabilities. Therefore, automated and accurate analysis of melanoma has become highly desirable in assisting dermatologists for improving their efficiency and objectivity when interpreting dermoscopic images in clinical practice [3].

Automatic skin lesion segmentation is an essential component in computer-aided diagnosis (CAD) of melanoma [4] [5]. However, this is a very challenging task due to significant variations in location, shape, size, color and texture across different patients. In addition, some dermoscopic images have low contrast between lesion and surrounding skin, and suffer from artifacts and intrinsic features such as hairs, frames, blood vessels and air bubbles. Existing lesion segmentation methods based on clustering, thresholding, region growing, or deformable models have shown limited success in solving this difficult problem when applying to a large amount of image data [3], [6], [7].

Recent development of deep learning has revolutionized the field of machine learning and computer vision. Deep learning

techniques, especially deep convolutional neural networks [8], have been rapidly adopted in various medical image analysis problems, including body recognition [9], lesion detection [10], image registration [11], segmentation [12] and classification [13]. In particular, Yu et al. [14] introduced a deep residual network with more than 50 layers for automatic skin lesion segmentation, in which several residual blocks [15] were stacked together to increase the representative capability of their model. In [16], Bi et al. proposed a multi-stage approach to combine the outputs from multiple cascaded fully convolutional networks (FCNs) to achieve a final skin lesion segmentation. In our recent study [17], we developed a fully automatic method for skin lesion segmentation by leveraging a 19-layer deep FCN that is trained end-to-end and does not rely on prior knowledge of the data. Furthermore, we designed a novel loss function based on Jaccard distance that is directly related to image segmentation task and eliminates the need of sample re-weighting. Experimental results showed that our method outperformed other state-of-the-art algorithms on two benchmark datasets - one is from ISBI 2016 challenge titled as *skin lesion analysis towards melanoma detection* [18], and the other is the PH2 dataset [19].

In this paper, we present a major extension of our previous work to further enhance our model in automatic skin lesion segmentation. Specifically, 1) we investigate the potential of using a deeper network architecture with smaller convolutional kernels such that the new model has increased discriminative capacity to handle a larger variety of image acquisition conditions; 2) besides Red-Green-Blue (RGB) channels, we also investigate the use of channels in other color spaces, such as Hue-Saturation-Value (HSV) and CIELAB [20], as additional inputs to our network that aim for a more efficient training while controlling over-fitting; 3) we evaluate the proposed framework on ISBI 2017 *Skin Lesion Analysis Towards Melanoma Detection* challenge¹ datasets. Experimental results demonstrated a significant performance gain as compared to our previous model, ranking itself as the first place among 21 final submissions.

II. DATASET AND PRE-PROCESSING

We solely used ISBI 2017 challenge datasets for training and validating the proposed deep learning model named as convolutional-deconvolutional neural network (CDNN). As compared to ISBI 2016 challenge, the image database in 2017 is doubled in size and includes a larger variety of tumor appearance on dermoscopic images, which makes the automatic

Y. Yuan and Y-C Lo are with the Department of Radiation Oncology, Icahn School of Medicine at Mount Sinai, New York, NY, USA, e-mail: yading.yuan@mssm.edu, yeh-chi.lo@mountsinai.org.

¹<https://challenge.kitware.com/#challenge/583f126bcad3a51cc66c8d9a>

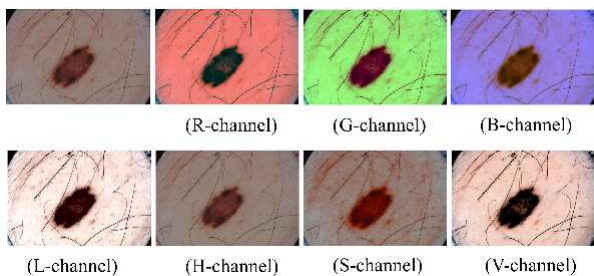


Fig. 1. The appearance of a dermoscopic image with color manipulation. The left image in the first row shows the original image, and the rest are the adjusted images by normalizing the contrast of each channel to [5, 95] percentile window, respectively.

lesion segmentation much more challenging. Specifically, the 2017 database includes a training dataset with 2000 annotated dermoscopic images (374 melanomas), and a blind held-out testing dataset with 600 images (117 melanomas). In order to facilitate model validation, a small independent dataset with 150 images (30 melanomas) is publicly available for challenge participants to fine tune the hyper-parameters before submitting the final results on the testing dataset. The image size ranges from 540×722 to 4499×6748 . By observing most of the images in the training set have a height to width ratio of 3 : 4, we resized all the images to 192×256 using bi-linear interpolation to keep balance between segmentation performance and computation cost.

While RGB is the most popular space to represent color information of natural images, its usage in image segmentation is however restricted by the fact that the RGB channels are not independent to each other. Thus, when applying image augmentation onto each channel during network training, the resultant image may have unrealistic appearance that makes the training less efficient. In order to address this issue and to use color information more effectively, we added the three channels from HSV color space and the lightness channel (L) from CIELAB color space, which separate *luma* (image intensity) from *chroma* (color information) to allow independent process on these two types of information. Figure 1 shows how a dermoscopic image can be adjusted by normalizing the contrast of each channel to [5, 95] percentile window. No other pre-processing was performed, so the input dimension to our CDNN model is $192 \times 256 \times 7$.

III. METHODS

The CDNN model we proposed belongs to FCNs category, which allows an entire image segmentation in a single pass instead of classifying the central pixel of a small image patch each time. Using an entire image as input not only makes model training and inference more efficient, but also includes much richer contextual information as compared to small patches, which usually leads to more robust and accurate segmentation.

A. CDNN model

In our previous work [17], we proposed a CDNN model containing 19 layer with 290, 129 trainable parameters. This

model consists of two pathways, in which the convolutional path resembles a traditional CNN that extracts a hierarchy of image features from low to high complexity, and the deconvolutional path transforms the aggregated features and reconstructs the segmentation map from coarse to fine resolution. In this way, CDNN can take both global information and fine details into account for tumor segmentation.

In order to improve the discriminative power of CDNN to handle a much larger variety of image acquisition conditions, we extend the previous model in the following two aspects. Firstly, we employ small 3×3 kernels in nearly all the convolutional and de-convolutional layers and maintain the same effective receptive field size of larger kernels by adding additional layers. This deeper architecture reduces the number of weights while allowing more non-linear transformations on the data. Then we increase the number of features in each layer in order to boost the capacity of the CDNN model. All convolutional and de-convolutional layers use Rectified Linear Units (ReLUs) as the nonlinear activation function [21], and batch normalization [22] is applied to reduce the internal covariate shift for each training mini-batch. The batch size was set as 18 in this study. Eventually the network contains 29 layers with 5, 042, 589 trainable parameters. The filter size and number of channels of the output feature maps are shown in Table I.

TABLE I
ARCHITECTURAL DETAILS OF THE PROPOSED CDNN MODEL
(ABBREVIATIONS: CONV: CONVOLUTIONAL LAYER; POOL: MAX-POOLING LAYER; DECV: DECONVOLUTIONAL LAYER, UPS: UPSAMPLING LAYER).

| Conv | Filter | Features | Deconv | Filter | Features |
|----------|--------------|----------|----------|--------------|----------|
| conv-1-1 | 3×3 | 16 | decv-1 | 3×3 | 256 |
| conv-1-2 | 3×3 | 32 | ups-1 | 2×2 | 256 |
| pool-1 | 2×2 | 32 | decv-2-1 | 3×3 | 256 |
| conv-2-1 | 3×3 | 64 | decv-2-2 | 3×3 | 128 |
| conv-2-2 | 3×3 | 64 | ups-2 | 2×2 | 128 |
| pool-2 | 2×2 | 64 | decv-3-1 | 4×4 | 128 |
| conv-3-1 | 3×3 | 128 | decv-3-2 | 3×3 | 128 |
| conv-3-2 | 4×4 | 128 | ups-3 | 2×2 | 128 |
| pool-3 | 2×2 | 128 | decv-4-1 | 3×3 | 64 |
| conv-4-1 | 3×3 | 256 | decv-4-2 | 3×3 | 32 |
| conv-4-2 | 3×3 | 256 | ups-4 | 2×2 | 32 |
| pool-4 | 2×2 | 256 | decv-5-1 | 3×3 | 16 |
| conv-5 | 3×3 | 512 | output | 3×3 | 1 |

The CDNN model represents an end-to-end mapping from the input image to a segmentation map, where each element is the probability that the corresponding input pixel belongs to the tumor. Those trainable parameters are learned from training data by minimizing a loss function. We use a loss function based on Jaccard distance [17]:

$$L_{d,j} = 1 - \frac{\sum_{i,j} (t_{ij} p_{ij})}{\sum_{i,j} t_{ij}^2 + \sum_{i,j} p_{ij}^2 - \sum_{i,j} (t_{ij} p_{ij})}, \quad (1)$$

where t_{ij} and p_{ij} are target and the output of pixel (i, j) , respectively. As compared to the conventionally used cross-entropy, the proposed loss function is directly related to image

segmentation task because Jaccard index is a common metric to assess medical image segmentation accuracy, especially in this ISBI 2017 challenge. Meanwhile, this loss function is well adapted to the problems with high imbalance between foreground and background classes as it doesn't require any class re-balancing.

Given a new test dermoscopic image, it is firstly rescaled to 192×256 with 7 color channels and the CDNN model is applied to yield a segmentation map. A dual-thresholds method is then developed to generate a binary tumor mask from the CDNN output. In this method, a relatively high threshold ($th_H = 0.8$) is firstly applied to determine the tumor center, which is calculated as the centroid of the region that has the largest mass among the candidates from thresholding. Then a lower threshold, $th_L = 0.5$, is applied to the segmentation map. After filling small holes with morphological dilation, the final tumor mask is determined as the region that embraces the tumor center.

B. Implementation details

Our CDNN model is implemented with Python using publicly available Theano [23] and Lasagne² packages. The model was trained from scratch using Adam stochastic optimization method [24] that adaptively adjusts the learning rate based on the first and the second-order moments of the gradient at each iteration. The initial learning rate α was set as 0.003.

In order to reduce overfitting, we add two dropout layers with $p = 0.5$ before conv-4-1 and decv-5-1 in Table I. In addition, we implement two types of image augmentation to further improve the robustness of the proposed model under a wide variety of image acquisition conditions. One consists of a series of geometric transformations, including randomly flipping, shifting, rotating as well as scaling. The other type focuses on randomly normalizing the contrast of each channels in the training images. Note that these augmentations only require little extra computation, so the transformed images are generated from the original images for every mini-batch with each iteration.

We used five-fold cross validation to evaluate the performance of our model on the challenge training dataset, in which a few hyper-parameters were also experimentally determined via grid search. The total number of iterations was set as 600 for each fold. When applying the trained models onto the testing dataset, a bagging-type ensemble strategy was implemented to average the outputs of the six models to further improve the segmentation performance. One iteration in model training took about 60 seconds using a single NVIDIA Geforce GTX 1060 GPU with 1280 cores and 6GB memory. Applying the entire segmentation framework on a new test image was, however, very efficient, taking about 0.2 second for a typical 768×1024 image.

²<http://github.com/Lasagne/Lasagne>

TABLE II
COMPARISON OF DIFFERENT ARCHITECTURES ON VALIDATION DATASET

| Image size | AC | DI | JA | SE | SP |
|------------|--------------|--------------|--------------|--------------|--------------|
| CDNN-19 | 0.945 | 0.839 | 0.749 | 0.854 | 0.982 |
| CDNN-29 | 0.953 | 0.865 | 0.783 | 0.879 | 0.979 |

TABLE III
COMPARISON OF DIFFERENT ARCHITECTURES ON TESTING DATASET

| Image size | AC | DI | JA | SE | SP |
|------------|--------------|--------------|--------------|--------------|--------------|
| CDNN-19 | 0.921 | 0.824 | 0.736 | 0.796 | 0.979 |
| CDNN-29 | 0.934 | 0.849 | 0.765 | 0.825 | 0.975 |

IV. EXPERIMENTS AND RESULTS

A. Evaluation metrics

We applied the challenge evaluation metrics to evaluate the performance of our method by comparing the computer-generated lesion masks with the ground truths created by human experts. The evaluation metrics include pixel-wise accuracy (AC), sensitivity (SE), specificity (SP), dice coefficient (DI), and Jaccard index (JA):

- $AC = (TP + TN) / (TP + FP + TN + FN)$
- $DI = 2 \cdot TP / (2 \cdot TP + FN + FP)$
- $JA = TP / (TP + FN + FP)$
- $SE = TP / (TP + FN)$
- $SP = TN / (TN + FP)$,

where TP , TN , FP , FN refer to the number of true positives, true negatives, false positives, and false negatives respectively. The final rank was based on JA for this challenge.

B. Experiments on network architectures

In order to investigate if the increase of network depth with smaller kernel size can improve the discriminative capability of CDNN and thus yield a better segmentation performance, we compared the performance of the proposed deep CDNN, which we denoted as CDNN-29, with the one proposed in our previous work, which we denoted as CDNN-19. Since only the results on the validation dataset could be obtained during the challenge, this comparison was initially conducted on the validation dataset, as shown in Table II. The ground truth of testing dataset was held out by the organizer for final performance evaluation during the challenge, and later released to the public to encourage further investigations. So we extended this comparison to the testing dataset in this experiment, as shown in Table III.

It is clear to see that the new CDNN model achieved better segmentation performance in most of the metrics on both validation and testing datasets. These results demonstrate that increasing network depth while maintaining equivalent receptive field by reducing filter size can effectively improve the discriminative capability of CDNN.

C. Experiments on input channels

Using CDNN-29 model, we evaluated how the additional HSV and L channels affect skin lesion segmentation performance. Figure 2 shows how the loss function is minimized as

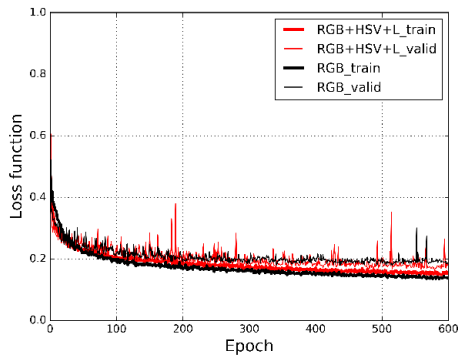


Fig. 2. Comparison of network inputs with and without the additional HSV+L color channels for training and validating of the proposed model.

TABLE IV

COMPARISON OF DIFFERENT INPUT CHANNELS ON VALIDATION DATASET

| Image size | AC | DI | JA | SE | SP |
|------------|--------------|--------------|--------------|--------------|--------------|
| RGB | 0.951 | 0.848 | 0.765 | 0.868 | 0.976 |
| RGB+HSV+L | 0.953 | 0.865 | 0.783 | 0.879 | 0.979 |

network training evolves. The black lines represent the model training and validation using RGB channels, and the red lines add additional four channels as model input. It is clear to see that the gap between training and validation errors was effectively narrowed down when including the additional four color channels as network input. Meanwhile, the validation error with additional color channels was consistently lower than that of RGB alone, yielding improved performance on the new testing images. As shown in Table IV and V, the additional four input channels improved the Jaccard index by 2.4% and 1.5% on validation and testing datasets, respectively.

D. Comparison with other methods in the challenge

During the 2017 ISBI challenge on skin lesion segmentation, 39 teams evaluated their algorithms during validation phase, but only 21 teams were able to participate the final official challenge by submitting their results on the 600 testing images. Table VI lists the results from the top ten teams. Because the previous studies have shown the advantage of using CNNs in skin lesion segmentation over other traditional methods [14], [17], most of the top teams in this challenge included various deep neural network models in their segmentation methods, with the exception that the NedMos team employed active contour on the saliency map [25]. While each team was allowed for multiple submissions, only the most recent one would be considered to determine the team's final score. Our method achieved an average Jaccard Index (JA) of 0.765, ranking as the first place in this challenge.

Figure 3 shows a few challenging examples of automatic skin lesion segmentation with our CDNN model, demonstrating the robustness of the proposed model under various imaging acquisition conditions.

V. DISCUSSIONS

While deep convolutional neural networks have shown remarkable success in various medical image segmentation

TABLE V

COMPARISON OF DIFFERENT INPUT CHANNELS ON TESTING DATASET

| Image size | AC | DI | JA | SE | SP |
|------------|--------------|--------------|--------------|--------------|--------------|
| RGB | 0.931 | 0.840 | 0.754 | 0.813 | 0.976 |
| RGB+HSV+L | 0.934 | 0.849 | 0.765 | 0.825 | 0.975 |

TABLE VI

RESULTS OF 2017 ISBI CHALLENGE ON SKIN LESION SEGMENTATION

| Team | AC | DI | JA | SE | SP |
|------------------|--------------|--------------|--------------|--------------|--------------|
| MtSinai (ours) | 0.934 | 0.849 | 0.765 | 0.825 | 0.975 |
| NLP LOGIX | 0.932 | 0.847 | 0.762 | 0.820 | 0.978 |
| USYD (Bi) | 0.934 | 0.844 | 0.760 | 0.802 | 0.985 |
| USYD (Ann) | 0.934 | 0.842 | 0.758 | 0.801 | 0.984 |
| RECOD | 0.931 | 0.839 | 0.754 | 0.817 | 0.970 |
| Jer | 0.930 | 0.837 | 0.752 | 0.813 | 0.976 |
| NedMos | 0.930 | 0.839 | 0.749 | 0.810 | 0.981 |
| INESC | 0.922 | 0.824 | 0.735 | 0.813 | 0.968 |
| Shenzhen U (Lee) | 0.922 | 0.810 | 0.718 | 0.789 | 0.975 |
| GAMMA | 0.915 | 0.797 | 0.715 | 0.774 | 0.970 |

tasks, it is still a challenging task to extend those models into a scaled-up study where a large amount of image data are involved. In this study, we investigated if a deeper CDNN model coupled with additional input information is capable of handling the increased complexity introduced from the much dynamic appearance of the targeting objects. It should be noted that deep neural networks have a very flexible architecture and different network design certainly matters. However, there is no clear guideline about what the optimal network architecture would be for a given application and available data. While it is infeasible to explore all the possible options in our study due to the long training time, we participated the ISBI 2017 challenge on skin lesion segmentation, which not only provides a large database to evaluate the performance of our model, but also allows researchers to compare different designs using the same benchmark data.

All of the top five teams employed deep learning in their segmentation methods, demonstrating the popularity and effectiveness of FCN-based methods in medical image segmentation. These methods cover a large spectrum of FCN models and training strategies. For example, Berseth from NLP LOGIX [26] employed a U-Net architecture [27] and tried to include a conditional random field (CRF) [28] as post-processing in their method. Besides the 2000 training images provided by the challenge organizers, Bi and Ann from USYD [29] trained their deep residual networks with additional ~ 8000 images from ISIC archive. We attribute the superior performance of our CDNN model to the following three aspects: 1) A deeper architecture with small kernel allowed more non-linear transformations on the data while reducing the number of trainable parameters as compared to its shallower counterpart, yielding significantly improved discriminant capability; 2) Additional input features made network training more efficient and robust by explicitly including complementary but useful information from other color spaces; 3) The loss function based on Jaccard distance enabled the network training to naturally focus more on lesion pixels over background, which further improved the segmentation performance by lifting sensitivity (SE), as demonstrated in

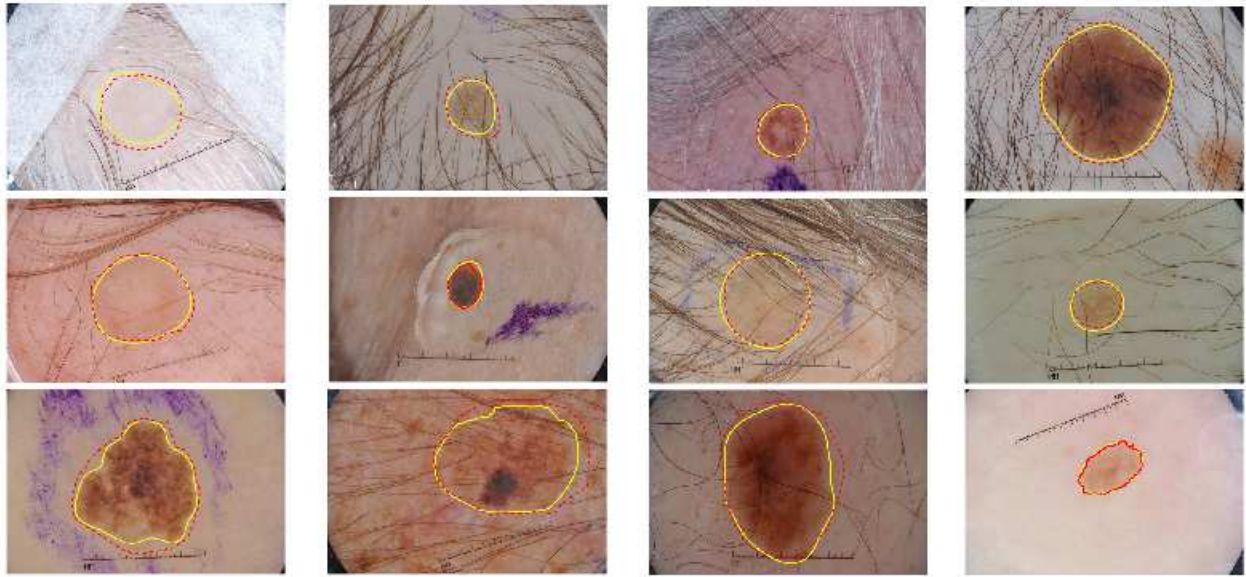


Fig. 3. Examples of automatic segmentation on the ISBI 2017 challenge testing dataset, including four nevus lesions in the top row, four seborrheic keratosis lesions in the middle rows and four melanoma lesions in the bottom row. In each figure, the red dash line indicates the outline contoured by dermatologist and the yellow solid line is the result of automatic segmentation.

Table VI.

The segmentation performance on some cases is still rather low, as shown in two examples in Figure 4. Thus, further improvement is certainly needed. In addition to better network architecture and more effective training strategies, one possible way is to combine the deep learning models with the conventional image segmentation methods, such as active contour. For example, we found the correlation between the outputs of our model and MedMos (active contour model) was 0.759, while it was 0.873 with NLP LOGIX (another deep FCN model). The scatter plots are shown as Figure 5. Since the active contour is less correlated with our model, it may provide more complementary information when ensembling multiple models for further segmentation. Another option is to integrate other post-processing techniques, such as CRF, into our CDNN model. We actually attempted to employ this technique in this challenge, but ultimately discard it due to the inferior performance. One possible reason is that the parameters to determine the unary and pairwise potentials were pre-set and thus lack of flexibility to handle the large variations of the data. A more dynamic mechanism, such as plugging CRF in as a part of FCN by modeling it as recurrent neural networks (RNNs) [30], may resolve this issue and thus improve the segmentation performance. These are all interesting research topics and worthy of further investigations.

VI. CONCLUSION

In this paper, we present a major extension of our previously proposed CDNN model in automatic skin lesion segmentation on dermoscopic images. Our new model leverages the increased discriminant capability of deeper network structures with smaller convolutional kernels to segment skin lesions in a much larger variety of image acquisition conditions. The

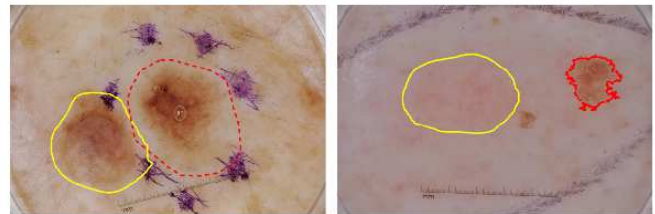


Fig. 4. Cases where our model failed due to mis-segmentation to the wrong sites. The red dash and yellow solid contours indicate the ground truth and the segmentation results, respectively.

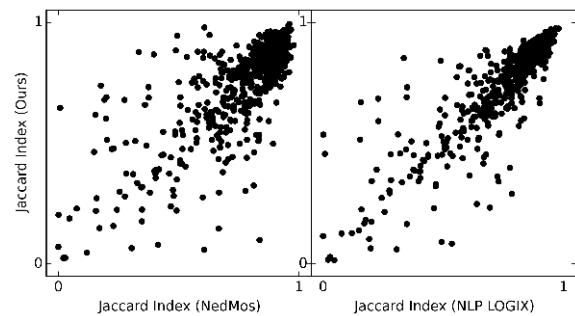


Fig. 5. Scatter plots of our model versus NedMos (left), and NLP LOGIX (right).

segmentation performance was further boosted by combining information from multiple color spaces. Our approach excelled other state-of-the-art methods when evaluating on ISBI 2017 challenge of skin lesion segmentation. Our network architectures and training strategies are inherently general and can be easily extended to other applications.

VII. ACKNOWLEDGMENT

The authors are grateful to the organizers of 2017 International Symposium on Biomedical Imaging (ISBI 2017) challenge of *Skin Lesion Analysis Towards Melanoma Detection* for organizing such an inspiring challenge.

REFERENCES

- [1] R. L. Siegel, K. D. Miller, and A. Jemal, "Cancer statistics, 2016," *CA Cancer J Clin.*, vol. 66, pp. 7–30, 2016.
- [2] M. Vestergaard, P. Macaskill, P. Holt, and S. Menzies, "Dermoscopy compared with naked eye examination for the diagnosis of primary melanoma: a meta-analysis of studies performed in a clinical setting," *Br. J. Dermatol.*, vol. 159, no. 3, pp. 669–676, 2008.
- [3] K. Korotkov and R. Garcia, "Computerized analysis of pigmented skin lesions: a review," *Artif. intell. Med.*, vol. 56, no. 2, pp. 69–90, 2012.
- [4] H. Ganster, P. Pinz, R. Rohrer, E. Wildling, M. Binder, and H. Kittler, "Automated melanoma recognition," *IEEE Trans. Med. Imag.*, vol. 20, no. 3, pp. 233–239, 2001.
- [5] M. E. Celebi, H. A. Kingravi, B. Uddin, H. Iyatomi, Y. A. Aslandogan, W. V. Stoecker, and R. H. Moss, "A methodological approach to the classification of dermoscopy images," *Comput. Med. Imag. Graph.*, vol. 31, no. 6, pp. 362–373, 2007.
- [6] M. Silveira, J. C. Nascimento, J. S. Marques, A. R. Marçal, T. Mendonça, S. Yamauchi, J. Maeda, and J. Rozeira, "Comparison of segmentation methods for melanoma diagnosis in dermoscopy images," *IEEE J. Sel. Top. Signal Process.*, vol. 3, no. 1, pp. 35–45, 2009.
- [7] M. E. Celebi, H. Iyatomi, G. Schaefer, and W. V. Stoecker, "Lesion border detection in dermoscopy images," *Comput. Med. Imag. Graph.*, vol. 33, no. 2, pp. 148–153, 2009.
- [8] Y. LeCun, L. Bottou, Y. Bengio, and P. Haffner, "Gradient-based learning applied to document recognition," *Proceedings of the IEEE*, vol. 86, no. 11, pp. 2278–2324, 1998.
- [9] Z. Yan, Y. Zhan, Z. Peng, S. Liao, Y. Shinagawa, S. Zhang, D. N. Metaxas, and X. S. Zhou, "Multi-instance deep learning: Discover discriminative local anatomies for bodypart recognition," *IEEE Trans. Med. Imag.*, vol. 35, no. 5, pp. 1332–1343, 2016.
- [10] D. C. Cireşan, A. Giusti, L. M. Gambardella, and J. Schmidhuber, "Mitosis detection in breast cancer histology images with deep neural networks," in *Proc. MICCAI 2013*. Springer, 2013, pp. 411–418.
- [11] S. Miao, Z. J. Wang, and R. Liao, "A CNN Regression Approach for Real-Time 2D/3D Registration," *IEEE Trans. Med. Imag.*, vol. 35, no. 5, pp. 1352–1363, 2016.
- [12] K. H. Cha, L. Hadjiiski, R. K. Samala, H.-P. Chan, E. M. Caoili, and R. H. Cohan, "Urinary bladder segmentation in CT urography using deep-learning convolutional neural network and level sets," *Med. Phys.*, vol. 43, no. 4, pp. 1882–1896, 2016.
- [13] A. Esteva, B. Kuprel, R. A. Novoa, J. Ko, S. M. Swetter, H. M. Blau, and S. Thrun, "Dermatologist-level classification of skin cancer with deep neural networks," *Nature*, vol. 542, no. 7639, pp. 115–118, 2017.
- [14] L. Yu, H. Chen, Q. Dou, J. Qin, and P. A. Heng, "Automated melanoma recognition in dermoscopy images via very deep residual networks," *IEEE Trans. Med. Imag.*, vol. 36, no. 4, pp. 994–1004, 2017.
- [15] K. He, X. Zhang, S. Ren, and J. Sun, "Deep residual learning for image recognition," in *CVPR 2016*. IEEE, 2016, pp. 770–778.
- [16] L. Bi, J. Kim, E. Ahn, A. Kumar, and D. Feng, "Dermoscopic image segmentation via multistage fully convolutional networks," *IEEE Trans. Biomed. Eng.*, vol. 64, no. 9, pp. 2065–2074, 2017.
- [17] Y. Yuan, M. Chao, and Y.-C. Lo, "Automatic skin lesion segmentation using deep fully convolutional networks with jaccard distance," *IEEE Trans. Med. Imaging*, vol. 36, no. 9, pp. 1876–1886, 2017.
- [18] D. Gutman, N. C. Codella, E. Celebi, B. Helba, M. Marchetti, N. Mishra, and A. Halpern, "Skin Lesion Analysis toward Melanoma Detection: A Challenge at the International Symposium on Biomedical Imaging (ISBI) 2016, hosted by the International Skin Imaging Collaboration (ISIC)," *arXiv preprint arXiv:1605.01397*, 2016.
- [19] T. Mendonça, P. M. Ferreira, J. S. Marques, A. R. Marçal, and J. Rozeira, "PH 2-A dermoscopic image database for research and benchmarking," in *Proc. EMBC 2013*. IEEE, 2013, pp. 5437–5440.
- [20] K. Plataniotis and A. N. Venetsanopoulos, *Color image processing and applications*. Springer Science & Business Media, 2013.
- [21] A. Krizhevsky, I. Sutskever, and G. E. Hinton, "Imagenet classification with deep convolutional neural networks," in *Adv. Neural Inf. Process. Sys.*, 2012, pp. 1097–1105.
- [22] S. Ioffe and C. Szegedy, "Batch normalization: Accelerating deep network training by reducing internal covariate shift," *arXiv preprint arXiv:1502.03167*, 2015.
- [23] T. T. D. Team, R. Al-Rfou, G. Alain, A. Almahairi, C. Angermueller, D. Bahdanau, N. Ballas, F. Bastien, J. Bayer, A. Belikov *et al.*, "Theano: A python framework for fast computation of mathematical expressions," *arXiv preprint arXiv:1605.02688*, 2016.
- [24] D. Kingma and J. Ba, "Adam: A method for stochastic optimization," *arXiv preprint arXiv:1412.6980*, 2014.
- [25] M. Jahanifar, N. Z. Tajeddin, A. Goodya, and B. M. Asl, "Segmentation of lesions in dermoscopy images using saliency map and contour propagation," *arXiv preprint arXiv:1703.00087*, 2017.
- [26] M. Berseth, "ISIC 2017 - Skin lesion analysis towards melanoma detection," *arXiv preprint arXiv:1703.00523*, 2017.
- [27] O. Ronneberger, P. Fischer, and T. Brox, "U-net: Convolutional networks for biomedical image segmentation," in *Proc. MICCAI 2015*. Springer, 2015, pp. 234–241.
- [28] L.-C. Chen, G. Papandreou, I. Kokkinos, K. Murphy, and A. L. Yuille, "Semantic image segmentation with deep convolutional nets and fully connected CRFs," *arXiv preprint arXiv:1412.7062*, 2014.
- [29] L. Bi, K. Kim, E. Ann, and D. Feng, "Automatic skin lesion analysis using large-scale dermoscopy images and deep residual networks," *arXiv preprint arXiv:1703.04197*, 2017.
- [30] S. Zheng, S. Jayasumana, B. Romera-Paredes, V. Vineet, Z. Su, D. Du, C. Huang, and P. Torr, "Conditional random fields as recurrent neural networks," in *ICCV*, 2015, pp. 1529–1537.